arXiv:cond-mat/0507305v1 [cond-mat.supr-con] 13 Jul 2005

Role of Spin-Orbit Coupling on the Spin Triplet Pairing in $\mathrm{Na_xCoO_2} \cdot y\mathrm{H_2O}$
I: d-vector under Zero Magnetic Field

Youichi Yanase*, Masahito Mochizuki and Masao Ogata

Department of Physics, University of Tokyo, Tokyo 113-0033

(Received Today 2005)

The d-vector in possibile spin triplet superconductor $\mathrm{Na_xCoO_2} \cdot y\mathrm{H_2O}$ is microscopically investigated on the basis of the multi-orbital Hubbard model including the atomic spin-orbit coupling. As a result of the perturbation theory, we obtain the stable spin triplet superconductivity where the p-wave and f-wave states can be stabilized. If we neglect the spin-orbit coupling, superconducting state has 6-fold (3-fold) degeneracy in the p-wave (f-wave) state. This degeneracy is lifted by the spin-orbit coupling. We determine the d-vector within the linearlized Dyson-Gorkov equation. It is shown that the d-vector is always along the plane when the pairing symmetry is p-wave, while it depends on the parameters in case of the f-wave state. The lifting of degeneracy is significant in the p-wave state while it is very small in the f-wave state. This is because the first order term with respect to the spin-orbit coupling is effective in the former case, while it is ineffective in the latter case. The consistency of these results with NMR and μSR measurements are discussed.

KEYWORDS: $\mathrm{Na_xCoO_2} \cdot y\mathrm{H_2O}$; spin triplet superconductivity; multi-orbital model; d-vector

1. Introduction

The unconventional superconductivity in strongly correlated systems has been one of the central issues in the condensed matter physics. For example, heavy fermion superconductors,[1] high-T_c cuprates,[2] organic superconductors[3] and $\mathrm{Sr_2RuO_4}$[4] are cited. Recently, a new superconductor $\mathrm{Na_xCoO_2} \cdot y\mathrm{H_2O}$ was discovered by Takada *et al*,[5] and the possibility of unconventional superconductivity has attracted huge interests.

Immediately after the discovery of superconductivity in $\mathrm{Na_xCoO_2} \cdot y\mathrm{H_2O}$, the symmetry of superconductivity has been studied by many experimental measurements.[6–18] While some controversial results exist,[16] most of them have indicated the non-s-wave superconductivity. For example, the absence of coherence peak in NMR $1/T_1T$[8,9] and the power low behaviors in $1/T_1T$[8,9] and specific heat[13–15] are evidences for the anisotropic pairing. Recently, a magnetic phase has been discovered in the neighborhood of superconducting phase.[19,20] This observation clearly indicates the importance of electron correlation which generally leads to the non-s-wave superconductivity.

These experimental indications have accelerated theoretical studies on the superconductivity in $\mathrm{Na_xCoO_2} \cdot y\mathrm{H_2O}$. In the first stage, the effect of frustration stimulated many interests since $\mathrm{Na_xCoO_2} \cdot y\mathrm{H_2O}$ has layered structure constructed by the triangular lattice. The RVB theory has been applied to the triangular lattice[21–24] and concluded the spin singlet d-wave superconductivity. Some authors have pointed out the frustration of charge ordering at the electron filling $n = 4/3$,[23] and the f-wave superconductivity due to the charge fluctuation has been discussed.[25,26] Recently, the RVB theory has been applied to the multi-orbital model and concluded the spin triplet superconductivity.[27]

Another theoretical approach is based on the perturbation expansion from the weak coupling region which includes the perturbation theory,[28] random phase approximation,[29] FLEX approximation[30] and perturbative renormalization group.[31] Some authors have taken account of the Fermi surface of $\mathrm{Na_xCoO_2} \cdot y\mathrm{H_2O}$ partly, and concluded the f-wave superconductivity,[30] g-wave superconductivity,[29] i-wave superconductivity[32] and nearly degeneracy between d- and f-wave superconductivities.[28]

Although these theories except for Refs. 27 and 29 have assumed single-orbital models, the conduction band in $\mathrm{Na_xCoO_2} \cdot y\mathrm{H_2O}$ has orbital degeneracy, as pointed out by Koshibae *et al.*[33] The conduction band mainly consists of three t_{2g}-orbitals in Co ions which hybridize with O2p-orbitals. Therefore, it is highly desired that the pairing symmetry in this material is examined on the basis of the multi-orbital model.

For this purpose, we have constructed a three-orbital Hubbard model which appropriately reproduces the electronic structure obtained in the LDA calculations,[34–36] and we have analyzed it on the basis of the FLEX approximation[37] and perturbation theory.[38] Then, we have obtained some notable results which are summarized as follows. (i) The spin triplet superconductivity is stable unless the Hund's rule coupling is very small. (ii) The p-wave state and f-wave state are nearly degenerate owing to the orbital degree of freedom. (iii) There is a nearly ferromagnetic spin correlation along the plane which stabilizes the spin triplet pairing. This is consistent with recent neutron scattering measurements which have reported the anti-ferromagnetic order with stacking ferromagnetic plane.[39] (iv) The vertex correction whose importance has been pointed out for $\mathrm{Sr_2RuO_4}$[40,41] is not important in $\mathrm{Na_xCoO_2} \cdot y\mathrm{H_2O}$. (v) The two of three orbitals, namely e'_g-doublet are essential for the superconductivity. The orbital-dependent-superconductivity proposed for $\mathrm{Sr_2RuO_4}$[42] is partly justified in $\mathrm{Na_xCoO_2} \cdot y\mathrm{H_2O}$. (vi) However, the orbital degeneracy in e'_g-doublet is particularly important because the single-orbital approximation artificially suppresses the p-wave superconductivity. This point is in sharp contrast to $\mathrm{Sr_2RuO_4}$ where the single-orbital approximation is valid.[40] In this sense, $\mathrm{Na_xCoO_2 \cdot \mathit{y}H_2O}$ is a typical multi-orbital superconductor in d-electron system.

One of the interesting subjects in the multi-orbital superconductor is the role of spin-orbit coupling. This issue is particularly important in the spin triplet superconductivity which has an internal degree of freedom described by the d-vector.[43, 44] If we neglect the spin-orbit coupling as in the previous studies,[37, 38] the 6-fold (3-fold) degeneracy remains in the p-wave (f-wave) state at $T = T_c$. Therefore, we have to take into account the spin-orbit coupling to determine the pairing state. The goal of this paper is to clarify the role of spin-orbit coupling and microscopically determine the d-vector in $\mathrm{Na_xCoO_2 \cdot \mathit{y}H_2O}$.

The d-vector is particularly important to discuss the Knight shift measurement which has been a powerful method to determine the pairing symmetry.[45] This is because the magnetic susceptibility in spin triplet superconductor significantly depends on the direction of d-vector. Although many experiments have been performed to determine the pairing symmetry in $\mathrm{Na_xCoO_2 \cdot \mathit{y}H_2O}$,[6–18] there is any conclusive evidence neither for the spin triplet pairing nor for the spin singlet pairing. We think that this is partly due to the lack of knowledges on the pairing state expected in the spin triplet superconductivity. The results in this paper will provide a clear subject for a comparison between the theory and experiment.

The role of spin-orbit coupling on the spin triplet superconductivity has been a longstanding problem since the discovery of heavy fermion superconductors.[44–49] However, the microscopic study has not been performed owing to the complicated electronic structure of heavy fermion systems. The discussion about the pairing symmetry in $\mathrm{UPt_3}$ still continues[47–49] partly because there is no microscopic research on the anisotropy of d-vector. Recently, we have developed a microscopic theory on the d-vector and applied to $\mathrm{Sr_2RuO_4}$.[50] The present study on $\mathrm{Na_xCoO_2 \cdot \mathit{y}H_2O}$ provides a contrasting example and we expect that these studies on the d-electron systems will lead to a systematic understanding including the f-electron systems.

This paper is organized as follows. In §2, we introduce the three-orbital Hubbard model including the atomic spin-orbit coupling and derive the two-orbital Hubbard model like in the previous study.[38] The pairing symmetry allowed in this model is classified in §3. The linearized Dyson-Gorkov equation in the multi-orbital model including the spin-orbit coupling is developed in §4.1. In §4.2, the pairing state is determined on the basis of the second order perturbation theory. We show that the role of spin-orbit coupling is quite different between the p-wave superconductivity and f-wave one. This difference is illuminated by showing the splitting of T_c in §4.3. We show that the d-vector in the p-wave state is strongly fixed against the magnetic field, while that in the f-wave state is fixed weakly. In §4.4, we discuss the cross-over from the weak spin-orbit coupling region $\lambda \ll W$ relevant for $\mathrm{Na_xCoO_2 \cdot \mathit{y}H_2O}$ to the strong spin-orbit coupling region $\lambda \gg W$. Although the latter is unrealistic for $\mathrm{Na_xCoO_2 \cdot \mathit{y}H_2O}$, this analysis will be useful for a unified understanding including the heavy fermion superconductors. In §5, we summarize the comparisons between $\mathrm{Na_xCoO_2 \cdot \mathit{y}H_2O}$ and $\mathrm{Sr_2RuO_4}$. Some discussions are given in the last section §6.

2. Spin-Orbit Coupling in Multi-Orbital Hubbard Model

First of all, we introduce a three-orbital Hubbard model including the spin-orbit coupling from which a two-orbital model are derived later. We consider a two-dimensional model which represents Co ions on the triangular lattice. We have constructed a tight-binding model for Co t_{2g}-orbitals which reproduces the results of LDA calculations.[37] By adding the spin-orbit coupling term and Coulomb interaction term, the three-orbital Hubbard model is obtained as,

$$H_3 = H_0 + H_{\mathrm{LS}} + H_{\mathrm{I}}, \tag{1}$$

$$H_0 = \sum_{i,j,s} \sum_{a,b} t_{a,b,i,j} c^{\dagger}_{i,a,s} c_{j,b,s}, \tag{2}$$

$$H_{\mathrm{LS}} = 2\lambda \sum_i \boldsymbol{L}_i \boldsymbol{S}_i, \tag{3}$$

$$\begin{aligned} H_{\mathrm{I}} = {} & U \sum_i \sum_a n_{i,a,\uparrow} n_{i,a,\downarrow} + U' \sum_i \sum_{a>b} n_{i,a} n_{i,b} \\ & - J_{\mathrm{H}} \sum_i \sum_{a>b} (2\boldsymbol{S}_{i,a}\boldsymbol{S}_{i,b} + \frac{1}{2} n_{i,a} n_{i,b}) \\ & + J \sum_i \sum_{a \neq b} c^{\dagger}_{i,a,\downarrow} c^{\dagger}_{i,a,\uparrow} c_{i,b,\uparrow} c_{i,b,\downarrow}. \end{aligned} \tag{4}$$

Here, the indices i and j denote the sites in the real space and indices a and b denote the orbitals. We assign the d_{xy}-, d_{yz}- and d_{xz}-orbitals to $a = 1$, $a = 2$ and $a = 3$, respectively.

The first term H_0 is a tight-binding Hamiltonian where $t_{a,b,i,j}$ are determined according to the symmetry of orbitals and lattice. The dispersion relation expected in the LDA calculation is reproduced by assuming nine hopping parameters from t_1 to t_9 as well as the crystal field splitting e_c which arises from the distortion of octahedron. For instance, we assume $t_{1,1,i,i\pm\mathbf{a}} = t_1$, $t_{1,1,i,i\pm\mathbf{b}} = t_2$, $t_{2,3,i,i\pm\mathbf{a}} = t_3$, $t_{1,1,i,i\pm(\mathbf{a}-\mathbf{b})} = t_4$, $t_{1,1,i,i\pm2\mathbf{a}} = t_5$, $t_{2,3,i,i\pm2\mathbf{a}} = t_6$, $t_{2,3,i,i\pm(\mathbf{a}-\mathbf{b})} = t_7$, $t_{1,3,i,i\pm(\mathbf{a}-\mathbf{b})} = t_8$ and $t_{1,2,i,i\pm(\mathbf{a}-\mathbf{b})} = t_9$. We denote the basis of triangular lattice as $\mathbf{a}=(\sqrt{3}/2,-1/2)$ and $\mathbf{b}=(0,1)$ and we choose the lattice constant as a unit length. The other hopping matrix elements $t_{a,b,i,j}$ are obtained by the symmetry operation. Since t_3 is largest among t_n, we choose the unit of energy as $t_3 = 1$ throughout this paper. We describe H_0 in the matrix representation as,

$$H_0 = \sum_{\boldsymbol{k},s} \hat{c}^{\dagger}_{\boldsymbol{k},s} \hat{H}(\boldsymbol{k}) \hat{c}_{\boldsymbol{k},s}, \tag{5}$$

where $\hat{c}^{\dagger}_{\boldsymbol{k},s} = (c^{\dagger}_{\boldsymbol{k},1,s}, c^{\dagger}_{\boldsymbol{k},2,s}, c^{\dagger}_{\boldsymbol{k},3,s})$ is a vector representation of Fourier transformed creation operators with spin s. The matrix element of $\hat{H}(\boldsymbol{k})$ has been given in Refs. 37

and 38.

In order to clarify the nature of superconductivity in this model, it is useful to introduce a non-degenerate a_{1g}-orbital and doubly-degenerate e'_{g}-orbitals. They are defined as,

$$|a_{1g}>=\frac{1}{\sqrt{3}}(|\mathrm{xy}>+|\mathrm{xz}>+|\mathrm{yz}>), \tag{6}$$

$$|e_{g},1>=\frac{1}{\sqrt{2}}(|\mathrm{xz}>-|\mathrm{xy}>), \tag{7}$$

$$|e_{g},2>=\frac{1}{\sqrt{6}}(2|\mathrm{yz}>-|\mathrm{xz}>-|\mathrm{xy}>). \tag{8}$$

The orbital-dependent-superconductivity in $\mathrm{Na_xCoO_2}\cdot y\mathrm{H_2O}$ occurs in this basis as shown in Refs. 37 and 38. We choose a basis of e'_{g}-orbitals different from Ref. 38 in order to simplify the following notations. By choosing the basis wave function as eqs. (6-8), the tight-binding Hamiltonian is transformed to be,

$$H_0=\sum_{\boldsymbol{k},s}\hat{d}^{\dagger}_{\boldsymbol{k},s}\hat{H}'(\boldsymbol{k})\hat{d}_{\boldsymbol{k},s}, \tag{9}$$

through the unitary transformation. Here, $\hat{d}^{\dagger}_{\boldsymbol{k},s}=(d^{\dagger}_{\boldsymbol{k},1,s},d^{\dagger}_{\boldsymbol{k},2,s},d^{\dagger}_{\boldsymbol{k},3,s})$ where $d^{\dagger}_{\boldsymbol{k},1,s}$, $d^{\dagger}_{\boldsymbol{k},2,s}$ and $d^{\dagger}_{\boldsymbol{k},3,s}$ are creation operators of $|a_{1g}>$, $|e_{g},1>$ and $|e_{g},2>$-orbitals, respectively.

We choose the c-axis as a quantization axis of spin for a convenience of following discussion. By choosing the basis functions as eqs. (6-8), we obtain a simplified expression for the atomic spin-orbit coupling term H_{LS} as,

$$H_{\mathrm{LS}}=\lambda\sum_{\boldsymbol{k}}\begin{pmatrix}\hat{d}^{\dagger}_{\boldsymbol{k},\uparrow} & \hat{d}^{\dagger}_{\boldsymbol{k},\downarrow}\end{pmatrix} \times\begin{pmatrix}0&0&0&0&\mathrm{i}&-1\\0&0&-\mathrm{i}&-\mathrm{i}&0&0\\0&\mathrm{i}&0&1&0&0\\0&\mathrm{i}&1&0&0&0\\-\mathrm{i}&0&0&0&0&\mathrm{i}\\-1&0&0&0&-\mathrm{i}&0\end{pmatrix}\begin{pmatrix}\hat{d}_{\boldsymbol{k},\uparrow}\\\hat{d}_{\boldsymbol{k},\downarrow}\end{pmatrix}. \tag{10}$$

Interestingly, the matrix element of eq. (10) is the same as that in $\mathrm{Sr_2RuO_4}$.[50,51] Therefore, we can discuss the role of spin-orbit coupling in $\mathrm{Na_xCoO_2}\cdot y\mathrm{H_2O}$ in analogy with $\mathrm{Sr_2RuO_4}$. Note that the basis wave function in $\mathrm{Sr_2RuO_4}$ is d_{xy}-, d_{yz}- and d_{zx}-orbitals, while that is $|a_{1g}>$, $|e_{g},1>$ and $|e_{g},2>$-orbitals in $\mathrm{Na_xCoO_2}\cdot y\mathrm{H_2O}$. This difference arises from the position of apex oxygens. While an apex of $\mathrm{RuO_6}$ octahedron is along the c-axis, all of apex oxygens in $\mathrm{CoO_6}$ octahedron are tilted from the c-axis. When we consider the matrix element in eq. (10), the d_{xy}-orbital in $\mathrm{Sr_2RuO_4}$ corresponds to the a_{1g}-orbital in $\mathrm{Na_xCoO_2}\cdot y\mathrm{H_2O}$, while the d_{yz}- and d_{zx}-orbitals correspond to the e'_{g}-doublet. It is expected that the d_{xy}-orbital is responsible for the superconductivity in $\mathrm{Sr_2RuO_4}$,[40,50] while the superconductivity is mainly caused by the e'_{g}-doublet in $\mathrm{Na_xCoO_2}\cdot y\mathrm{H_2O}$.[37,38] Thus, these two materials provide contrasting examples of spin triplet superconductors.

The coupling constant 2λ in H_{LS} has been estimated as 57mev.[52] This value corresponds to $\lambda=0.17$ in our unit if we choose the band width $W\sim 9t_3=1.5$eV according to the LDA calculations. Since this estimation has some ambiguities, we investigate the range from $\lambda=0.05$ to $\lambda=0.25$. In this range, the effect of spin-orbit coupling on the band structure is very small. There is a hole pocket enclosing the Γ-point and six hole pockets near the K-points, which are consistent with LDA calculations.[34–36] The former (a_{1g}-Fermi surface) mainly consists of the a_{1g}-orbital and the latter (e_{g}-Fermi surface) mainly consists of the e'_{g}-orbitals.

From the analysis of three-orbital Hubbard model with $\lambda=0$,[37,38] we have found that the superconductivity is mainly induced by the e'_{g}-orbitals and the a_{1g}-orbital can be simply ignored to discuss qualitative features of superconductivity. Therefore, we derive a two-orbital Hubbard model by simply dropping the a_{1g}-orbital as,

$$H_2=H_0^{(2)}+H_{\mathrm{I}}^{(2)}, \tag{11}$$

$$H_0^{(2)}=\sum_{\boldsymbol{k},s}\hat{a}^{\dagger}_{\boldsymbol{k},s}\hat{H}^{(2)}(\boldsymbol{k},s)\hat{a}_{\boldsymbol{k},s}, \tag{12}$$

$$\begin{aligned}H_{\mathrm{I}}^{(2)}=&\,U\sum_{i}\sum_{a=1}^{2}n_{i,a,\uparrow}n_{i,a,\downarrow}+U'\sum_{i}\sum_{a>b}n_{i,a}n_{i,b}\\&-J_{\mathrm{H}}\sum_{i}\sum_{a>b}(2\boldsymbol{S}_{i,a}\boldsymbol{S}_{i,b}+\frac{1}{2}n_{i,a}n_{i,b})\\&+J\sum_{i}\sum_{a\neq b}a^{\dagger}_{i,a,\downarrow}a^{\dagger}_{i,a,\uparrow}a_{i,b,\uparrow}a_{i,b,\downarrow}.\end{aligned} \tag{13}$$

Here, we have introduced a two component vector $\hat{a}^{\dagger}_{\boldsymbol{k},s}=(d^{\dagger}_{\boldsymbol{k},2,s},d^{\dagger}_{\boldsymbol{k},3,s})$ and 2×2 matrix

$$\hat{H}^{(2)}(\boldsymbol{k},s)=\begin{pmatrix}e'_{11}(\boldsymbol{k}) & e'_{12}(\boldsymbol{k})-\mathrm{i}s\lambda\\ e'_{21}(\boldsymbol{k})+\mathrm{i}s\lambda & e'_{22}(\boldsymbol{k})\end{pmatrix}. \tag{14}$$

Here, $e'_{ij}(\boldsymbol{k})$ is obtained from eq. (9) as $e'_{ij}(\boldsymbol{k})=\hat{H}'(\boldsymbol{k})_{i+1,j+1}$ where $\hat{H}'(\boldsymbol{k})_{i,j}$ is the matrix element of $\hat{H}'(\boldsymbol{k})$. It should be noticed that the off-diagonal matrix elements connecting up and down spins in eq. (10) vanish. This means that the operators L_{x} and L_{y} have no matrix element in the Hilbert space expanded by e'_{g}-orbitals. Therefore, only the spin-orbit coupling along the z-axis is effective in the two-orbital model. This fact remarkably simplifies the calculation and provides a clear understanding for the results in §4.

The second term in eq. (11) describes the on-site Coulomb interactions including the intra-orbital repulsion U, inter-orbital repulsion U', Hund's rule coupling J_{H} and pair hopping term J. We impose the relations $U=U'+J_{\mathrm{H}}+J$ and $J_{\mathrm{H}}=J$ throughout this paper. The Coulomb interaction term is invariant for the unitary transformation with respect to the orbital owing to these relations.

In this paper, we investigate the d-vector in $\mathrm{Na_xCoO_2}\cdot y\mathrm{H_2O}$ on the basis of the two-orbital Hubbard model in eq. (11). According to Refs. 37 and 38, we choose the hopping parameters as,

$(t_1,t_2,t_4,t_5,t_6,t_7,t_8,t_9)=$

$$a(0.1, 0.2, 0.3, -0.2, -0.05, 0.2, 0.2, -0.25). \quad (15)$$

where $a = 0.6 \sim 1$ is consistent with LDA calculations. We choose a small value of $a = 0.6$ in this paper. This is because the electric DOS in $e_{\rm g}$-Fermi surface decreases by neglecting the $a_{\rm 1g}$-orbital and this artificial decrease is compensated by decreasing a. We define the number of holes in the two-orbital model as $n_{\rm e}$ which corresponds to the area of $e_{\rm g}$-Fermi surface. According to the chemical analysis,[53,54] the total number of holes is $n = 0.4 \sim 0.5$ which is different from $n = 0.67$ in the parent material $\rm Na_{0.33}CoO_2$. Since $0 \le n_{\rm e} \le n$, we investigate the range $n_{\rm e} = 0.05 \sim 0.35$. We have found that $n_{\rm e}$ is an important parameter for the superconductivity rather than n.[38] The superconducting instability is significantly suppressed when $n_{\rm e} = 0$. For finite $n_{\rm e}$, the superconducting $T_{\rm c}$ slightly increases with the increase of crystal field splitting $e_{\rm c}$ which leads to the increase of $n_{\rm e}$.[38,55] The recent NMR measurement has confirmed an important role of $e_{\rm c}$.[19] We show a typical Fermi surface of two-orbital model in Fig. 1.

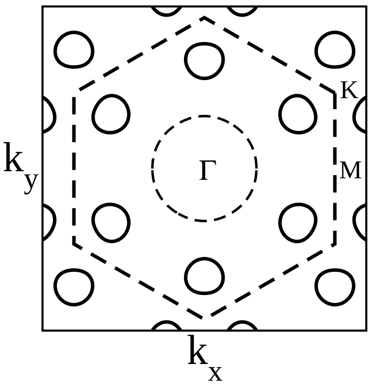

Fig. 1. Fermi surface in the two-orbital Hubbard model (solid lines). We have shown the Fermi surface of $a_{\rm 1g}$-orbital which is determined as $\hat{H}'(\boldsymbol{k})_{11} - \mu = 0$ (thin dashed line). The thick dashed line is the first Brillouin zone of triangular lattice. The parameters are chosen to be $\lambda = 0.17$, $a = 0.6$, $n_{\rm e} = 0.21$ and $n = 0.5$.

It should be noted that ARPES measurements[56,57] for non-superconducting $\rm Na_{\it x}CoO_2$ observed the $a_{\rm 1g}$-Fermi surface, but the $e_{\rm g}$-Fermi surface has not been found. This observation implies $n_{\rm e} = 0$ which contradicts with our basic assumption, namely a finite value of $n_{\rm e}$. Our analysis on the three-orbital Hubbard model has shown that the superconductivity is hardly stabilized when $n_{\rm e} = 0$.[38] This result implies that the $e_{\rm g}$-Fermi surface exists in the superconducting materials as expected in LDA calculations. The increase of $n_{\rm e}$ is actually expected in superconducting materials because the $\rm H_2O$ molecules increase the crystal field splitting $e_{\rm c}$, as shown by the NMR measurement.[19]

3. Classification of the Pairing State

Before the microscopic analysis, we classify the symmetry of pairing state in the two-orbital Hubbard model including the spin-orbit coupling. First, we show the orbital part of spin triplet pairing function in Table I. There are two wave functions in both p-wave symmetry and f-wave symmetry. The $p_{\rm x}$-wave and $p_{\rm y}$-wave are degenerate owing to the symmetry of triangular lattice. On the other hand, the f_1-wave and f_2-wave are not degenerate.

$\rm E_1$	$p_{\rm x}$-wave	$\sin \frac{\sqrt{3}}{2}k_{\rm x} \cos \frac{1}{2}k_{\rm y}$
	$p_{\rm y}$-wave	$\sin k_{\rm y} + \sin \frac{1}{2}k_{\rm y} \cos \frac{\sqrt{3}}{2}k_{\rm x}$
$\rm B_1$	f_1-wave	$\sin \frac{1}{2}k_{\rm y}(\cos \frac{1}{2}k_{\rm y} - \cos \frac{\sqrt{3}}{2}k_{\rm x})$
$\rm B_2$	f_2-wave	$\sin \frac{\sqrt{3}}{2}k_{\rm x}(\cos \frac{3}{2}k_{\rm y} - \cos \frac{\sqrt{3}}{2}k_{\rm x})$

Table I. Orbital part of odd-parity pairing function in the triangular lattice. The first column shows the irreducible representations of $\rm D_6$-group. The second column shows the notations adopted in this paper, which are the counterparts of the isotropic system. The third column shows the typical wave function. Note that the wave function obtained in the Dyson-Gorkov equation is different from the third column to some extent.

The spin part of pairing function is described by the d-vector as,[43,44]

$$\begin{pmatrix} \Delta_{\uparrow\uparrow}(k) & \Delta_{\uparrow\downarrow}(k) \\ \Delta_{\downarrow\uparrow}(k) & \Delta_{\downarrow\downarrow}(k) \end{pmatrix} = {\rm i}\hat{d}(k)\hat{\sigma}\sigma_y$$
$$= \begin{pmatrix} -d_{\rm x}(k) + {\rm i}d_{\rm y}(k) & d_{\rm z}(k) \\ d_{\rm z}(k) & d_{\rm x}(k) + {\rm i}d_{\rm y}(k) \end{pmatrix}. \quad (16)$$

Since the Cooper pair has spin $S = 1$, there is a 3-fold degeneracy in the $SU(2)$ symmetric system. Therefore, if the spin-orbit coupling is neglected, the degeneracy in the p-wave state is $3 \times 2 = 6$-fold due to the spin part and orbital part, while that in the f-wave state is 3-fold.

$P_{\rm xy+}$	$p_{\rm x}\hat{x} + p_{\rm y}\hat{y}$, $p_{\rm y}\hat{x} - p_{\rm x}\hat{y}$
$P_{\rm xy-}$	$p_{\rm x}\hat{x} - p_{\rm y}\hat{y}$, $p_{\rm y}\hat{x} + p_{\rm x}\hat{y}$
$P_{\rm z}$	$(p_{\rm x} \pm {\rm i}p_{\rm y})\hat{z}$
$F_{\rm xy}$	$f_1\hat{x} - \alpha f_2\hat{y}$, $\alpha f_2\hat{x} + f_1\hat{y}$
$F_{\rm z}$	$f_1\hat{z}$

Table II. Classification of the pairing state including the spin-orbit coupling. The first column shows the notations adopted in this paper.

Table II shows the classification of pairing state for finite spin-orbit coupling. According to the results for $\lambda = 0$,[38] the f_2-wave state is not stabilized in the multi-orbital Hubbard model. Therefore, we have not shown the pairing state which is reduced to the f_2-wave state in the limit $\lambda \to 0$. Since the spin-orbit coupling $\lambda < 0.25$ is much smaller than the band width $W \sim 9$, $|\alpha|$ in $F_{\rm xy}$-state is much smaller than 1.

The $F_{\rm xy}$-state and all of the p-wave states in Table II are two-dimensional representations. Although the two pairing states in $P_{\rm xy+}$ are not degenerate in general,[44] there remains an additional degeneracy in the two-orbital Hubbard model. This is because the matrix element of $L_{\rm x}$ and $L_{\rm y}$ vanishes in this model. The symmetry of Hubbard Hamiltonian with $\lambda = 0$ is $G \otimes SU(2) \otimes T \otimes U(1)$, where G, $SU(2)$, T and $U(1)$ show the symmetries of point group, spin rotation, time-reversal and gauge transformation, respectively. When the spin-orbit coupling exists, the symmetry is reduced to $G \otimes U(1) \otimes T \otimes U(1)$.

Thus, the $SU(2)$ symmetry is violated by the spin-orbit coupling. However, the $U(1)$ symmetry for the spin rotation in the plane remains because $L_{\rm x} = L_{\rm y} = 0$. This additional $U(1)$ symmetry is the origin of degeneracy in $P_{\rm xy+}$-state. In the three-orbital Hubbard model (eq. (4)), the symmetry is reduced to $G \otimes T \otimes U(1)$, and the degeneracy in the $P_{\rm xy+}$-state is lifted. However, it is expected that the lifting of degeneracy is small because the order parameter in $a_{\rm 1g}$-orbital is very small.[37,38]

4. Determination of the Pairing State

4.1 Linearized Dyson-Gorkov equation without $SU(2)$ symmetry

In this section, we determine the pairing state in the two-orbital Hubbard model by solving the linearized Dyson-Gorkov equation within the second order perturbation theory. The derivation of Dyson-Gorkov equation has been explained in literatures.[41] The application to the multi-orbital model including the spin-orbit coupling has been given in the study of $\mathrm{Sr_2RuO_4}$.[50] The application to the two-orbital model (eq. (11)) is simpler than that to $\mathrm{Sr_2RuO_4}$ because the transverse component of spin-orbit coupling vanishes.

In order to make following discussions clear, we introduce a unitary matrix $\hat{U}(\boldsymbol{k}, s) = (u_{ij}(\boldsymbol{k}, s))$ which diagonalizes $\hat{H}^{(2)}(\boldsymbol{k}, s)$, namely,

$$\hat{U}^{\dagger}(\boldsymbol{k}, s)\hat{H}^{(2)}(\boldsymbol{k}, s)\hat{U}(\boldsymbol{k}, s) = \begin{pmatrix} E_1(\boldsymbol{k}) & 0 \\ 0 & E_2(\boldsymbol{k}) \end{pmatrix}. \quad (17)$$

Here, $E_1(\boldsymbol{k}) \leq E_2(\boldsymbol{k})$ and $E_i(\boldsymbol{k})$ do not depend on the spin owing to the time-reversal symmetry and inversion symmetry. The Green function $\hat{G}(k, s) = ({\rm i}\omega_n \hat{1} - \hat{H}^{(2)}(\boldsymbol{k}, s))^{-1}$ is obtained as,

$$G_{ij}(k, s) = \sum_{\alpha=1}^{2} u_{i\alpha}(\boldsymbol{k}, s) u^{*}_{j\alpha}(\boldsymbol{k}, s) G_{\alpha}(k), \quad (18)$$

where $G_{\alpha}(k) = \frac{1}{{\rm i}\omega_n - E_{\alpha}(\boldsymbol{k})}$.

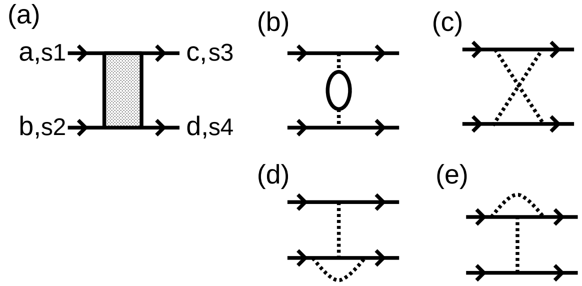

Fig. 2. (a) Diagrammatic representation of the irreducible vertex in the particle-particle channel. (b-e) The second order terms with respect to the Coulomb interactions (dashed lines). The solid line denotes the Green function having the indices of spin and orbital.

As shown in the LDA calculations, the energy band described by $E_2(\boldsymbol{k})$ crosses the Fermi level and $E_1(\boldsymbol{k})$ is far below the Fermi level. In this case, the superconducting transition is induced by the Cooper pairing in the $E_2(\boldsymbol{k})$-band. Therefore, the linearized Dyson-Gorkov equation is written in terms of an effective interaction within the $E_2(\boldsymbol{k})$-band,

$$\lambda_{\rm e}\Delta_{s1s2}(k) = -\sum_{k', s3, s4} V(k, k', s1, s2, s3, s4) \times |G_2(k')|^2 \Delta_{s3s4}(k'), \quad (19)$$

with

$$V(k, k', s1, s2, s3, s4) = \sum_{abcd} u^{*}_{a2}(\boldsymbol{k}, s1) u^{*}_{b2}(-\boldsymbol{k}, s2) \times V_{abcd}(k, k', s1, s2, s3, s4) u_{c2}(\boldsymbol{k}', s3) u_{d2}(-\boldsymbol{k}', s4). \quad (20)$$

Here, $V_{abcd}(k, k', s1, s2, s3, s4)$ is the irreducible vertex in the particle-particle channel having the indices of orbital and spin (see Fig. 2(a)). Because of $L_{\rm x} = L_{\rm y} = 0$, the z-component of spin is conserved and $V(k, k', s1, s2, s3, s4)$ is finite only if $s1 + s2 = s3 + s4$. Therefore, the linearized Dyson-Gorkov equation is reduced to the eigenvalue equations for $\Delta_{\uparrow\uparrow}$, $\Delta_{\uparrow\downarrow}$ and $\Delta_{\downarrow\downarrow}$, respectively.

$$\lambda_{\rm e}^{\uparrow\uparrow}\Delta_{\uparrow\uparrow}(k) = -\sum_{k'} V_{\uparrow\uparrow}(k, k')|G_2(k')|^2 \Delta_{\uparrow\uparrow}(k'), \quad (21)$$

$$\lambda_{\rm e}^{\uparrow\downarrow}\Delta_{\uparrow\downarrow}(k) = -\sum_{k'} V_{\uparrow\downarrow}(k, k')|G_2(k')|^2 \Delta_{\uparrow\downarrow}(k'), \quad (22)$$

$$\lambda_{\rm e}^{\downarrow\downarrow}\Delta_{\downarrow\downarrow}(k) = -\sum_{k'} V_{\downarrow\downarrow}(k, k')|G_2(k')|^2 \Delta_{\downarrow\downarrow}(k'), \quad (23)$$

where $V_{\uparrow\uparrow}(k, k') = V(k, k', \uparrow, \uparrow, \uparrow, \uparrow)$, $V_{\downarrow\downarrow}(k, k') = V(k, k', \downarrow, \downarrow, \downarrow, \downarrow)$ and $V_{\uparrow\downarrow}(k, k') = V(k, k', \uparrow, \downarrow, \uparrow, \downarrow) + V(k, k', \uparrow, \downarrow, \downarrow, \uparrow)$. It is notable that the maximum eigenvalues of eqs. (21) and (23) are equivalent. The wave functions are related to be $\Delta_{\downarrow\downarrow}(k) = e^{{\rm i}\phi}\Delta^{*}_{\uparrow\uparrow}(k)$ where the phase ϕ is arbitrary.

If we neglect the spin-orbit coupling, the maximum eigenvalue does not depend on the direction of d-vector since $V_{\uparrow\uparrow}(k, k') = V_{\downarrow\downarrow}(k, k') = V_{\uparrow\downarrow}(k, k')$. However, we find $\lambda_{\rm e}^{\uparrow\uparrow} = \lambda_{\rm e}^{\downarrow\downarrow} \neq \lambda_{\rm e}^{\uparrow\downarrow}$ when λ is finite. The superconducting transition is determined by the criterion, $\max(\lambda_{\rm e}^{\uparrow\uparrow}, \lambda_{\rm e}^{\uparrow\downarrow}) = 1$. If $\lambda_{\rm e}^{\uparrow\uparrow} > \lambda_{\rm e}^{\uparrow\downarrow}$, the $P_{\rm xy+}$-, $P_{\rm xy-}$- or $F_{\rm xy}$-state is stabilized at $T = T_{\rm c}$, while $P_{\rm z}$- or $F_{\rm z}$-state is stabilized when $\lambda_{\rm e}^{\uparrow\uparrow} < \lambda_{\rm e}^{\uparrow\downarrow}$.

In this paper, we estimate irreducible vertex $V_{abcd}(k, k', s1, s2, s3, s4)$ up to the second order with respect to the Coulomb interaction term $H_{\rm I}^{(2)}$. The diagrammatic representation is shown in Figs. 2(b-e) which are calculated from the possible combination of Coulomb interactions and Green functions. We numerically solve the eigenvalue equations for $\lambda_{\rm e}^{\uparrow\uparrow}$ and $\lambda_{\rm e}^{\uparrow\downarrow}$ and determine the pairing state with highest $T_{\rm c}$. In the following, we divide the first Brillouin zone into 128×128 lattice points and we take 512 Matsubara frequencies for $T \geq 0.005$ and 1024 Matsubara frequencies for $0.002 \leq T < 0.005$. We have confirmed that this size of calculation is sufficient for the following results.

4.2 d-vector

First, we show the phase diagram of two-orbital Hubbard model without spin-orbit coupling which will be a basis of following discussions. Figure 3 shows the stable pairing symmetry in the phase diagram of $n_{\rm e}$ and $J_{\rm H}$. In the figure, the intra-orbital repulsion U is determined so as to obtain $T_{\rm c} = 0.01$ which corresponds to 20K in our unit. This temperature is higher than the observed transition temperature $T_{\rm c} \sim 5$K. However, the stable pairing symmetry is almost independent of the temperature as shown in Ref. 38.

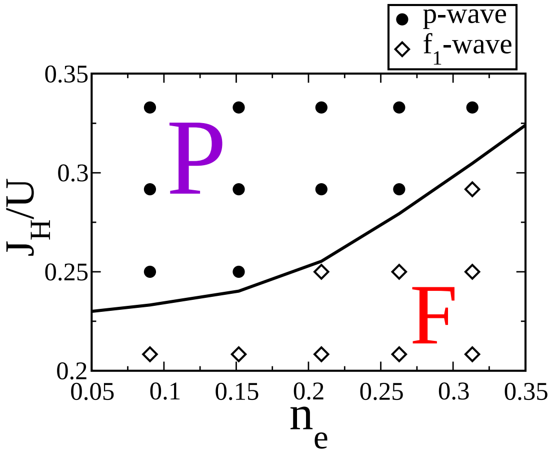

Fig. 3. Phase diagram without spin-orbit coupling in the $n_{\rm e}$-$J_{\rm H}$ plane. The solid line is the phase boundary obtained by the interpolation.

Among many parameters in the multi-orbital Hubbard model, the relevant parameter for the pairing symmetry is the Hund's rule coupling $J_{\rm H}$ and the number of holes in $e_{\rm g}$-Fermi surface $n_{\rm e}$.[38] Figure 3 is quite similar to the phase diagram of three-orbital model shown in Ref. 38. When the Hund's rule coupling is large and/or $n_{\rm e}$ is small, the p-wave superconductivity is stabilized. The f-wave superconductivity is stabilized for small $J_{\rm H}$ and/or large $n_{\rm e}$. The only qualitative difference between the two-orbital and three-orbital models is that the f-wave state stabilized for $n_{\rm e} < 0.1$ and $J_{\rm H}/U > 0.2$ in Ref. 38 vanishes in Fig. 3.

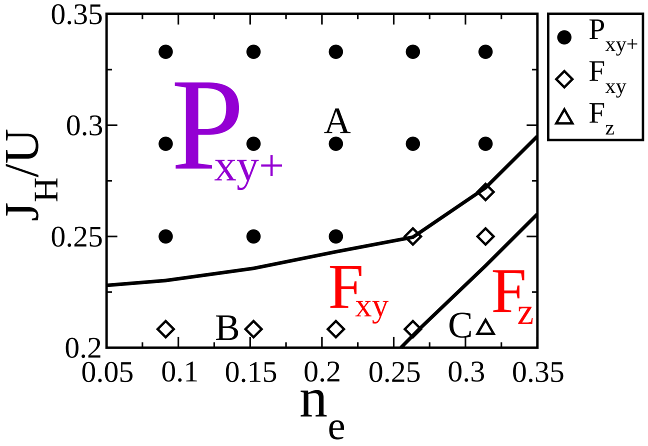

Fig. 4. Phase diagram including the spin-orbit coupling $\lambda = 0.17$. The notations of $P_{\rm xy+}$, $F_{\rm xy}$ and $F_{\rm z}$ have been given in Table II. The solid line is the phase boundary obtained by the interpolation.

We show the results of d-vector in Fig. 4, where the $T_{\rm c}$ is fixed to be $T_{\rm c} = 0.003 \sim 6$K consistent with experimental value. Hereafter, the parameter U is determined so as to obtain this $T_{\rm c}$. For example, we obtain $U = 6.57$, $U = 5.47$ and $U = 4.34$ in A, B and C in Fig. 4, respectively. It is clearly shown that the spin-orbit coupling stabilizes the $P_{\rm xy+}$-state when the pairing symmetry is p-wave. Then, the d-vector is parallel to the plane. On the other hand, the d-vector in the f-wave symmetry depends on the parameters, although the $F_{\rm xy}$-state seems to be most stable.

In order to understand these results, it is useful to analyze the role of spin-orbit coupling in a perturbative way. Although we have included the spin-orbit coupling term into the unperturbed Hamiltonian, the perturbative treatment is valid since λ is much smaller than the band width. As a result of perturbation expansion in λ, the effective interaction $V_{ss'}(k,k')$ is written as,

$$V_{ss'}(k,k') = V^{(0)}(k,k') + \sum_{n=1}^{\infty} \lambda^n V_{ss'}^{(n)}(k,k'). \tag{24}$$

We have actually applied this perturbation theory to $\rm Sr_2RuO_4$ and shown that the first order term vanishes when the γ-band is mainly superconducting.[50] This is because the hybridization term disappears between $d_{\rm xy}$-orbital and $d_{\rm yz}$- $d_{\rm zx}$-orbitals. However, the first order term exists in case of $\rm Na_xCoO_2 \cdot \mathit{y}H_2O$ since the large hybridization term exists in the $e'_{\rm g}$-doublet.

It is easy to find that the first order term always appears with the combination to the off-diagonal Green function or off-diagonal matrix element of $\hat{U}(\boldsymbol{k}, s)$. Taking into account the symmetry of $e'_{12}(\boldsymbol{k})$ in eq. (14), namely $e'_{12}(k_{\rm x}, k_{\rm y}) = -e'_{12}(-k_{\rm x}, k_{\rm y}) = -e'_{12}(k_{\rm x}, -k_{\rm y})$, we obtain the following relations,

$$V_{\uparrow\uparrow}^{(1)}(k,k') = V_{\downarrow\downarrow}^{(1)*}(k,k'), \tag{25}$$

$$\begin{aligned} V_{\uparrow\uparrow}^{(1)}(k_{\rm x}, k_{\rm y}, k'_{\rm x}, k'_{\rm y}) &= -V_{\uparrow\uparrow}^{(1)}(-k_{\rm x}, k_{\rm y}, -k'_{\rm x}, k'_{\rm y}) \\ &= -V_{\uparrow\uparrow}^{(1)}(k_{\rm x}, -k_{\rm y}, k'_{\rm x}, -k'_{\rm y}), \end{aligned} \tag{26}$$

$$V_{\uparrow\downarrow}^{(1)}(k,k') = 0. \tag{27}$$

According to eq. (26), the kernel of linearized Dyson-Gorkov equation works on the $p_{\rm x}$-wave state to produce the $p_{\rm y}$-wave state, namely

$$\sum_{k,k'} \Delta_{\rm y}(k) V_{\uparrow\uparrow}^{(1)}(k,k') |G_2(k')|^2 \Delta_{\rm x}(k') \neq 0, \tag{28}$$

and

$$\begin{aligned} &\sum_{k,k'} \Delta_{\rm x}(k) V_{\uparrow\uparrow}^{(1)}(k,k') |G_2(k')|^2 \Delta_{\rm x}(k') = \\ &\sum_{k,k'} \Delta_{\rm y}(k) V_{\uparrow\uparrow}^{(1)}(k,k') |G_2(k')|^2 \Delta_{\rm y}(k') = 0, \end{aligned} \tag{29}$$

where $\Delta_{\rm x}(k)$ and $\Delta_{\rm y}(k)$ are functions having the symmetry of $p_{\rm x}$-wave and $p_{\rm y}$-wave, respectively. Thus, the first order term in λ works like a first order perturbation on the degenerate states, namely $p_{\rm x}$- and $p_{\rm y}$-states. Therefore, the eigenvalue $\lambda_{\rm e}^{\uparrow\uparrow}$ for one of the $P_{\rm xy+}$- and $P_{\rm xy-}$-states increases in the first order of λ, while $\lambda_{\rm e}^{\uparrow\uparrow}$

for the other state decreases. On the other hand, the first order term vanishes for the d-vector along the c-axis according to eq. (27). Therefore, the d-vector along the plane is always stabilized within the first order theory in λ independent of the microscopic details. Which state is stabilized between $P_{\rm xy+}$ and $P_{\rm xy-}$ is determined by the microscopic calculation for $V_{ss'}(k,k')$. Figure 4 shows that the $P_{\rm xy+}$-state is stable within the second order perturbation theory.

The situation is quite different for the f-wave superconductivity. Owing to eq. (26), the first order term is not effective in the f_1-wave state, namely

$$\sum_{k,k'} \Delta_{\rm f1}(k) V^{(1)}_{\uparrow\uparrow}(k,k') |G_2(k')|^2 \Delta_{\rm f1}(k') = 0, \qquad (30)$$

where $\Delta_{\rm f1}(k)$ is the function having the f_1-wave symmetry. Although the first order term couples the f_1-wave state to the f_2-wave state, this is a higher order effect because these states are non-degenerate. Indeed, the eigenvalue of linearized Dyson-Gorkov equation for the f_2-wave state is much smaller than that for the f_1-wave state.[38] Then, the role of first order term, $V^{(1)}_{\uparrow\uparrow}(k,k')$ is negligibly small. Therefore, the direction of d-vector is determined by the higher order terms beyond the second order, namely $V^{(n)}_{ss'}(k,k')$ $(n \geq 2)$. The role of higher order terms depends on the microscopic details as we have shown in the case of $\rm Sr_2RuO_4$.[50] In $\rm Na_xCoO_2 \cdot \mathit{y}H_2O$, $F_{\rm xy}$-state ($F_{\rm z}$-state) is stabilized for small (large) value of $n_{\rm e}$ and/or large (small) value of $J_{\rm H}$ as shown in Fig. 4.

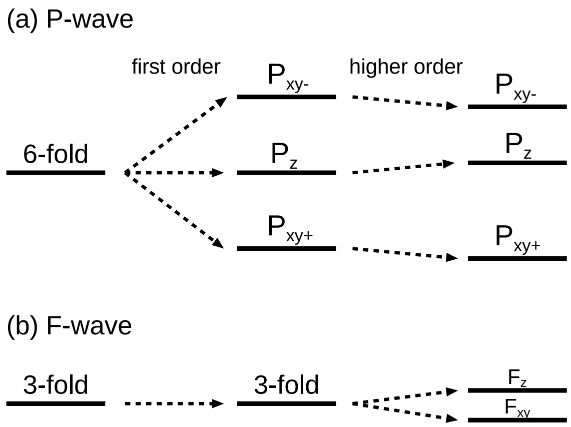

Fig. 5. Schematic figure of level scheme for (a) p-wave superconductivity and (b) f-wave superconductivity. The degeneracy at $\lambda = 0$ is shown on the left. The level splitting due to the first order perturbation in λ is shown in the center. The energy levels affected by the higher order perturbation are shown on the right. We assume in (b) that the $F_{\rm xy}$-state is stable rather than the $F_{\rm z}$-state.

We summarize the above discussions in Fig. 5. In case of the p-wave superconductivity, the first order perturbation in λ stabilizes the $P_{\rm xy+}$-state and destabilizes the $P_{\rm xy-}$-state. The $P_{\rm z}$-state is not affected in this order. We find that higher order perturbation terms favor the $P_{\rm xy+}$-state furthermore, as shown in Fig. 5(a). In case of the f-wave superconductivity, three-fold degeneracy is not lifted by the first order perturbation. The higher order perturbation stabilizes the $F_{\rm xy}$-state or $F_{\rm z}$-state depending on the parameters such as $J_{\rm H}$ and $n_{\rm e}$.

4.3 Splitting of $T_{\rm c}$

The quite different role of spin-orbit coupling between the p- and f-wave symmetries discussed above is illuminated by showing the splitting of $T_{\rm c}$. In eqs. (21-23), the linearized Dyson-Gorkov equation is defined for each direction of d-vector. We define the superconducting $T_{\rm c}$ for $\hat{d} \parallel xy$ and that for $\hat{d} \parallel z$ by the criterion $\lambda_{\rm e}^{\uparrow\uparrow}(T_{\rm c}^{\rm (xy)}) = 1$ and $\lambda_{\rm e}^{\uparrow\downarrow}(T_{\rm c}^{\rm (z)}) = 1$, respectively. The former corresponds to the $T_{\rm c}$ of $P_{\rm xy+}$- or $F_{\rm xy}$-state while the latter is the $T_{\rm c}$ of $P_{\rm z}$- or $F_{\rm z}$-state.

Figure 6 shows the splitting of $T_{\rm c}$, namely $\Delta T_{\rm c}/T_{\rm c} = |T_{\rm c}^{\rm (xy)} - T_{\rm c}^{\rm (z)}|/T_{\rm c}$. The parameters $J_{\rm H}$ and $n_{\rm e}$ are chosen to be A, B, C in Fig. 4, where the $P_{\rm xy+}$-state, $F_{\rm xy}$-state and $F_{\rm z}$-state are stable, respectively. It is clearly shown that $\Delta T_{\rm c}$ is much smaller in the f-wave symmetry than in the p-wave symmetry. This is because the first order term in λ is ineffective. Indeed, while $\Delta T_{\rm c}/T_{\rm c}$ increases linearly in the p-wave symmetry, the increase in the f-wave symmetry is nearly proportional to the square of λ.

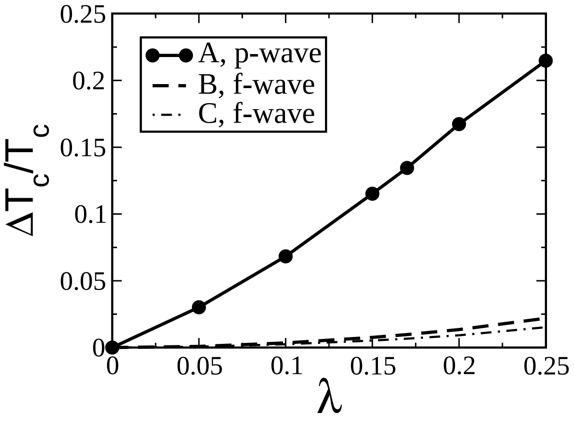

Fig. 6. λ-dependence of $\Delta T_{\rm c}/T_{\rm c} = |T_{\rm c}^{\rm (xy)} - T_{\rm c}^{\rm (z)}|/T_{\rm c}$. The parameters are chosen to be A, B and C in Fig. 4. The $P_{\rm xy+}$-state, $F_{\rm xy}$-state and $F_{\rm z}$-state are stable, respectively.

The quite different magnitude of $\Delta T_{\rm c}/T_{\rm c}$ shown in Fig. 6 will be reflected in the phase diagram under the magnetic field. In order to gain the Zeeman coupling energy, the d-vector can be rotated by the applied magnetic field. Fig. 6 indicates that the d-vector is strongly fixed against the magnetic field in case of the p-wave symmetry, however the d-vector in the f-wave symmetry rotates in a weak magnetic field. We have actually determined the phase diagram under the magnetic field on the basis of the weak coupling theory and found that the rotation does not occur in the p-wave symmetry up to the half of Pauli paramagnetic limit.[58] The results for the multiple phase diagram under the magnetic field and the characteristics of each phase will be shown in the subsequent publication.[58]

The results of Figs. 4 and 6 are important for an interpretation of NMR and μSR results because the magnetic susceptibility has an anisotropy arising from the direction of d-vector.[43,44] In general, the magnetic susceptibility in the unitary state is obtained as,

$$\chi_{\mu\nu}/\chi_{\rm n} = \\ < \delta_{\mu\nu} - (d_\mu(\boldsymbol{k}) d_\nu(\boldsymbol{k})/|\hat{d}(\boldsymbol{k})|^2)(1 - Y(\boldsymbol{k},T)) >_{\rm F}, \quad (31)$$

where $<>_{\rm F}$ is an average on the Fermi surface, $< A >_{\rm F} = \rho(0)^{-1} \int A \delta(E_2(\boldsymbol{k})) {\rm d}k$. Here, $\chi_{\rm n}$ is the magnetic susceptibility in the normal state, and $Y(\boldsymbol{k},T)$ is the angle dependent Yosida function,

$$Y(\boldsymbol{k},T) = \int_{-\infty}^{\infty} {\rm d}\xi (-\frac{{\rm d}f(E)}{{\rm d}E}))|_{E=\sqrt{\xi^2+|\hat{d}(k)|^2}}, \quad (32)$$

where $f(E)$ is the Fermi distribution function. It should be noticed that the magnetic susceptibility decreases for the magnetic field parallel to the d-vector. For the $P_{\rm xy+}$-state, it is reasonable to assume that $\hat{d} = p_{\rm x}\hat{x} + p_{\rm y}\hat{y}$ or $\hat{d} = p_{\rm y}\hat{x} - p_{\rm x}\hat{y}$ is stabilized below $T_{\rm c}$ among any linear combinations of these states. This is because the condensation energy is maximally gained in these states within the weak coupling theory. Then, the susceptibility along the plane $\chi_{\rm ab}$ decreases to the half of its value in the normal state, as shown in Fig. 7. In order to obtain Fig. 7, we have assumed the order parameter below $T_{\rm c}$ as $\hat{d}(\boldsymbol{k}) = \Delta(T)(\phi_{\rm x}(\boldsymbol{k})\hat{x} + \phi_{\rm y}(\boldsymbol{k})\hat{y})$ where $\phi_{\rm x}(\boldsymbol{k})$ and $\phi_{\rm y}(\boldsymbol{k})$ are obtained in eq. (21) as $\Delta_{\uparrow\uparrow}(\boldsymbol{k}, {\rm i}\pi T_{\rm c}) = -\phi_{\rm x}(\boldsymbol{k}) + {\rm i}\phi_{\rm y}(\boldsymbol{k})$. The wave functions $\phi_{\rm x}(\boldsymbol{k})$ and $\phi_{\rm y}(\boldsymbol{k})$ have the symmetry of $p_{\rm x}$-wave and $p_{\rm y}$-wave, respectively. We have calculated the temperature dependence of $\Delta(T)$ by using the effective model having the separable pairing interaction and solving it within the BCS theory. The same procedure has been used in Ref. 59. For the $F_{\rm xy}$-state, the in-plane magnetic field favors one of the degenerate states. For example, $\hat{d} = \alpha f_2 \hat{x} + f_1 \hat{y}$ is favored by the magnetic field along x-axis. Then, $\chi_{\rm ab}$ decreases owing to the induced f_2-wave component, however the decrease is very small as shown in Fig. 7 because $|\alpha| \ll 1$. Here, we have calculated the temperature dependence of order parameter in the same way as for the $P_{\rm xy+}$-state. The susceptibility along c-axis $\chi_{\rm c}$ does not decrease in both $P_{\rm xy+}$- and $F_{\rm xy}$-states. Although $\chi_{\rm c}$ decreases to zero in the $F_{\rm z}$-state at $T = 0$, the observation of this decrease will be difficult because the d-vector rotates in a very weak magnetic field.

The Knight shift below $T_{\rm c}$ has been measured by some groups.[6,7,10,60,61] Most of the measurements have been performed under the magnetic field parallel to the plane. It has been reported that the Knight shift in Co-NMR and O-NMR decreases below $T_{\rm c}$ in a weak magnetic field.[6,7,60,61] This observation is consistent with the $P_{\rm xy+}$-state in our results. The $P_{\rm xy+}$-state is furthermore consistent with the μSR measurement[10] which does not detect any time-reversal symmetry breaking expected in the $P_{\rm z}$-state and $d_{\rm x^2-y^2} + {\rm i}d_{\rm xy}$-state. Contrary to the other NMR measurements, the Knight shift in D-NMR is almost temperature independent below $T_{\rm c}$.[6] Although this observation is incompatible with the other NMR measurements, this is consistent with $F_{\rm xy}$- and $F_{\rm z}$-states in our calculation.

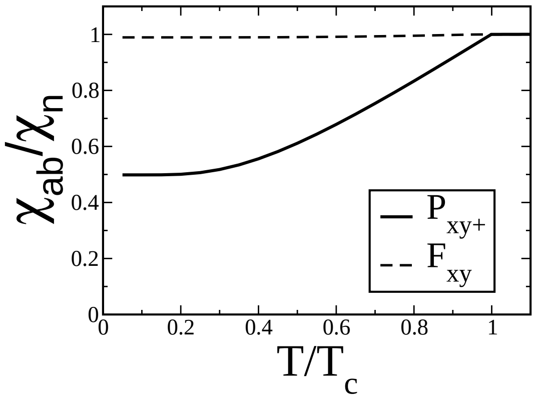

Fig. 7. Temperature dependence of magnetic susceptibility along the plane $\chi_{\rm ab}$ divided by the normal state value $\chi_{\rm n}$. We consider the magnetic field along x-axis and assume $\hat{d} = p_{\rm x}\hat{x} + p_{\rm y}\hat{y}$ in the $P_{\rm xy+}$-state and $\hat{d} = \alpha f_2 \hat{x} + f_1 \hat{y}$ in the $F_{\rm xy}$-state. We obtain the Fermi surface and momentum dependence of order parameter for the parameters A and B in Fig. 4, respectively.

4.4 Crossover from $\lambda \ll W$ to $\lambda \gg W$

In §4.1-3, we have considered the spin-orbit coupling much smaller than the band width, namely $\lambda \ll W$. This relation is expected in most of the d-electron systems including ${\rm Na_xCoO_2} \cdot y{\rm H_2O}$. On the other hand, the situation is opposite in the f-electron systems which include odd-parity superconductors. It is not clear whether the role of spin-orbit coupling is qualitatively different between the weak coupling region $\lambda \ll W$ and strong coupling region $\lambda \gg W$. Therefore, it is interesting to investigate global behaviors of two-orbital Hubbard model from $\lambda \ll W$ to $\lambda \gg W$, although the strong coupling region $\lambda \gg W$ is unrealistic for ${\rm Na_xCoO_2} \cdot y{\rm H_2O}$.

In Fig. 8, we show the anisotropy of eigenvalues of linearized Dyson-Gorkov equation $\lambda_{\rm an} = \lambda_{\rm e}^{\uparrow\downarrow}/\lambda_{\rm e}^{\uparrow\uparrow}$. The small value of $\lambda_{\rm an}$ means that the splitting of superconducting $T_{\rm c}$ is large. It is shown that the splitting of $T_{\rm c}$ takes its maximum for an intermediate value of λ. Thus, the anisotropy of d-vector decreases with increasing the spin-orbit coupling in the strong coupling region $\lambda \gg W$ in contrast to the weak coupling region. This behavior is quite different from the anisotropy of spin susceptibility $\chi_{\rm an} = \chi_{\rm c}/\chi_{\rm ab}$ which has been shown in Fig. 8 for a comparison. The anisotropy of spin susceptibility is enhanced monotonically with increasing the spin-orbit coupling, as expected.[62] Note that the structure around $\lambda = 2$ is due to the rapid change of Fermi surface. There are two hole pocket Fermi surfaces enclosing the K-point for $\lambda > 2$.

It is easy to understand the behavior of $\lambda_{\rm an}$ by taking the limit $\lambda \to \infty$ in advance. In this limit, the two-orbital Hubbard model is reduced to the single-orbital Hubbard model written as,

$$H_1 = \sum_{\boldsymbol{k},s} E_2(\boldsymbol{k}) c^\dagger_{\boldsymbol{k},s} c_{\boldsymbol{k},s} + \frac{U+U'}{2} \sum_i n_{i,\uparrow} n_{i,\downarrow}, \quad (33)$$

where the Coulomb interaction is renormalized to $\frac{U+U'}{2}$. It is notable that s in eq. (33) is not the spin but the

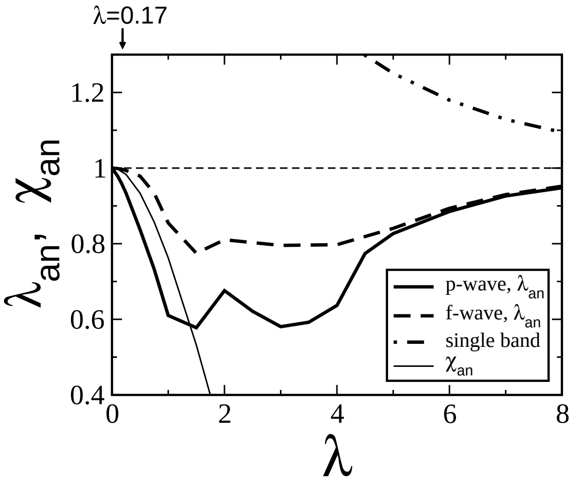

Fig. 8. The anisotropy of eigenvalues of linearized Dyson-Gorkov equation, $\lambda_{\rm an} = \lambda_{\rm e}^{\uparrow\downarrow}/\lambda_{\rm e}^{\uparrow\uparrow}$ in a wide range of spin-orbit coupling. The solid (dashed) line shows the result for the p-wave (f-wave) symmetry. The parameters are $J_{\rm H}/U = 7/24$, $e_{\rm c} = 0$, ($J_{\rm H}/U = 5/24$, $e_{\rm c} = -0.5$) and $T = 0.01$. Here, we fix the crystal field splitting $e_{\rm c}$ and total hole density $n = 0.5$ instead of $n_{\rm e}$. The anisotropy of spin susceptibility $\chi_{\rm an} = \chi_{\rm ab}/\chi_{\rm c}$ is shown by the thin solid line. The double dotted line shows $\lambda_{\rm e}^{\rm s}/\lambda_{\rm e}^{\uparrow\uparrow}$ where $\lambda_{\rm e}^{\rm s}$ is the eigenvalue in the single-orbital Hubbard model (eq. (33)).

pseudo-spin. This single-orbital model has the $SU(2)$ symmetry for the rotation of pseudo-spin. Therefore, spin triplet superconducting state is isotropic for the direction of d-vector defined by the pseudo-spin. In Fig. 8, we see that $\lambda_{\rm an}$ in the two-orbital model comes to unity in the limit $\lambda \rightarrow \infty$. Then, the maximum eigenvalue of linearized Dyson-Gorkov equation actually comes to that of single-orbital Hubbard model. On the other hand, the g-factor of Zeeman coupling term is anisotropic for the pseudo-spin, and therefore the anisotropy of spin susceptibility remains in the single-orbital model. In other words, the effect of spin-orbit coupling is absorbed by the character of quasi-particles and the residual interaction is isotropic in the strong coupling limit $\lambda \rightarrow \infty$.

Although the two-orbital Hubbard model in eq. (11) is too simple to provide a general formula, the same situation is generally expected when the heavy quasi-particles consist of one Kramers doublet. Actually, it has been reported by the NMR measurements[63] that the d-vector in UPt$_3$ is almost isotropic, although the spin susceptibility is significantly anisotropic. Thus, the anisotropy of d-vector and that of spin susceptibility is quite different in general.

5. Comparison with Sr$_2$RuO$_4$

Interestingly, we have found some similar aspects between Na$_{\rm x}$CoO$_2$ $\cdot$ yH$_2$O and Sr$_2$RuO$_4$. The latter is the most established spin triplet superconductor in d-electron systems.[4] One of the similarity is the orbital dependent superconductivity. The three $t_{2\rm g}$-orbitals is divided to two groups, namely $d_{\rm xy}$-orbital and $d_{\rm yz}$-$d_{\rm zx}$-orbitals in Sr$_2$RuO$_4$, $a_{1\rm g}$-orbital and $e'_{\rm g}$-orbitals in Na$_{\rm x}$CoO$_2$ $\cdot$ yH$_2$O. The superconductivity is mainly induced by the former in Sr$_2$RuO$_4$ while by the latter in Na$_{\rm x}$CoO$_2$ $\cdot$ yH$_2$O. Another interesting finding is that the spin-orbit coupling term has the same matrix element as eq. (10). This enables us to summarize the results on the d-vector in a unified way as shown in Table III.

Sr$_2$RuO$_4$		Na$_{\rm x}$CoO$_2$ $\cdot$ yH$_2$O	
Square lattice		Triangular lattice	
$d_{\rm xy}$	$d_{\rm yz}$, $d_{\rm zx}$	$e'_{\rm g}$	
$L_{\rm x}$, $L_{\rm y}$	$L_{\rm z}$	$L_{\rm z}$	
p-wave		p-wave	f-wave
O(λ^2)	O(λ)	O(λ)	O(λ^2)
$\hat{d}$ $\parallel$z	$\hat{d}$ $\parallel$xy	$\hat{d}$ $\parallel$xy	both

Table III. An unified description on the d-vector between Sr$_2$RuO$_4$ and Na$_{\rm x}$CoO$_2$ $\cdot$ yH$_2$O. The second column shows the symmetry of crystal. The third column shows the orbitals leading to the superconductivity. The forth column shows the important component of orbital moment. The fifth column shows the symmetry of superconductivity. The sixth column shows the leading order term with respect to the spin-orbit coupling. The last column shows the direction of d-vector. The results on Sr$_2$RuO$_4$ have been obtained in Ref. 50.

We also show the case where the $d_{\rm yz}$- and $d_{\rm zx}$-orbitals induce the superconductivity in Sr$_2$RuO$_4$. In this case, the results on the d-vector are qualitatively the same as the p-wave superconductivity in Na$_{\rm x}$CoO$_2$ $\cdot$ yH$_2$O. Actually, the analysis of the first order term in λ (see §4.2) can be applied to the case in Sr$_2$RuO$_4$ in the same way.[50] In both cases, the orbital moment along the c-axis stabilizes the d-vector along the plane.

The first order term in λ vanishes in Sr$_2$RuO$_4$ when the $d_{\rm xy}$-orbital is active. Although this is similar to the f-wave state in Na$_{\rm x}$CoO$_2$ $\cdot$ yH$_2$O, the microscopic origin is quite different. The first order term disappears in Sr$_2$RuO$_4$ since the hybridization term with $d_{\rm yz}$- and $d_{\rm zx}$-orbitals vanishes.[50]

Note that the results on Sr$_2$RuO$_4$ are consistent with experiments. It is believed that the $d_{\rm xy}$-orbital is mainly superconducting in Sr$_2$RuO$_4$. Then, we obtain the chiral superconducting state,[50] namely $P_{\rm z}$-state in Table II, which is consistent with the μSR measurement.[64] Owing to the disappearance of the first order term in λ, the d-vector can be rotated by a weak magnetic field along the c-axis. Actually, the NMR measurement has detected a d-vector along the plane under the weak magnetic field $H \parallel c$.[65]

6. Summary and Discussions

In this paper, we have investigated the d-vector in the possible spin triplet superconductor Na$_{\rm x}$CoO$_2$ $\cdot$ yH$_2$O on the basis of the two-orbital Hubbard model representing the $e'_{\rm g}$-orbitals. There remains a 6-fold (3-fold) degeneracy in the p-wave (f-wave) superconducting state if we neglect the spin-orbit coupling. Therefore, we include the L-S coupling term in Co ions into the Hamiltonian and determine the pairing state on the basis of the second order perturbation theory.

We find that the role of spin-orbit coupling is quite different between the p-wave superconductivity and f-wave superconductivity. The d-vector is always along the plane if the orbital part has the p-wave symmetry. On the other hand, the direction of d-vector depends on the parameters if the orbital part has the f-wave symmetry. In our calculation, the superconducting T_c is determined for each direction of d-vector. We show that the splitting of T_c in the p-wave state is much larger than that in the f-wave state.

Such a different role of spin-orbit coupling is explained by analyzing the first order term with respect to the spin-orbit coupling λ. This term is effective in the p-wave symmetry, but ineffective in the f-wave symmetry. This property is hold in all of the perturbation terms with respect to the Coulomb interactions. Therefore, the results in this paper will be valid beyond the second order perturbation theory adopted here. The only assumption is that the superconductivity is mainly induced by the e'_g-orbitals.

The determination of d-vector is especially important for the interpretation of Knight shift measurements because the magnetic properties of spin triplet superconductor depend on the direction of d-vector. Our results indicate that the d-vector can be rotated by a weak magnetic field in the case of f-wave superconductivity, while the d-vector is strongly fixed against the applied field in the case of p-wave superconductivity. The NMR Knight shift along the plane will decrease in the latter case because the d-vector has both $\hat{x}$ and $\hat{y}$ components. On the other hand, the Knight shift will be almost temperature-independent in the former case in all directions of applied magnetic field. Unfortunately, experimental results seem to be confusing. The NMR Knight shift in Co-site 6,7,60,61) and O-site 60) has shown a sizable decrease for the parallel magnetic field. This is consistent with our results for the p-wave state. On the other hand, the Knight shift in D-site has reported a qualitatively different result6) which is consistent with our results for the f-wave state.

Finally, we suggest some future experimental studies which are highly desired. First, the NMR Knight shift along c-axis may provide conclusive evidence for the pairing symmetry. Kobayashi *et al.* has reported a pioneering result which shows a slight decrease of Knight shift below T_c.7) Although this observation implies the spin singlet superconducting state, the theoretical interpretation seems not to be conclusive. It is noted that the decrease of c-axis Knight shift in Ref. 7 is very small compared with that of in-plane Knight shift. Although this small decrease may be explained on the basis of the vortex state with spin singlet pairing,7) another theoretical interpretation may be also valid. For example, we suggest three possibilities based on the spin triplet superconducting state. The first one is the coexistence of p- and f-wave superconductivities which will be discussed in the subsequent paper.58) Extending the present theory to determine the pairing state below T_c, we find this coexistent state around the boundary between the p- and f-wave states in Fig. 4. The magnetic susceptibility decreases in this state for all directions of magnetic field. The second one is the role of strong electron correlation. The conclusions obtained in the weak coupling BCS theory can be modified in the strongly correlated electron systems, especially near the magnetic instability. The third one is the role of disorder which leads to the rotation of d-vector. The detailed measurements of c-axis Knight shift including the magnetic field dependence, sample dependence and impurity effect are highly desired for a clear identification of the pairing state.

Second, the search for the multiple phase transition under the magnetic field is particularly interesting in the future study. The phase transition accompanied by a rotation of d-vector is expected in the spin triplet superconductor under the magnetic field. Such a phase transition is promising when the H_{c2} is large, namely when the magnetic field is applied along the plane. We have actually determined the phase diagram under the parallel magnetic field on the basis of the weak coupling theory.58) We find that such a phase transition is expected in the p-wave superconducting state and $p+f$ coexistent state while that is not expected in the f-wave state. Interestingly, the second phase in the p-wave state is different from all of the pairing states in Table II, and the NMR Knight shift decreases even in this phase. The results on this subject will be reported in another publication.58)

Third, the precise measurement on the critical field H_{c2} along the plane is important. Although some authors have reported the measurement, the results are controversial.17,18) If the H_{c2} far exceeds the Pauli paramagnetic limit, the spin triplet pairing state is promising. This issue is closely related to the second issue, namely the possibility of multiple phase transition. For example, it has been reported that the Knight shift in the Co-NMR and μSR does not decrease in a high magnetic field along the plane.6,10) If this magnetic field is still below H_{c2}, the qualitatively different behavior from the low magnetic field region indicates a multiple phase transition.

At last, it is desirable to determine the Fermi surface of superconducting material experimentally. Although the existence of e_g-Fermi surface is a basic assumption of this paper, it is not clear whether the e_g-Fermi surface exists or not. Recent ARPES measurements56,57) on the non-superconducting material have reported a qualitatively different Fermi surface from the LDA calculations.34–36) We think that the measurement on the superconducting material is highly desired.

Acknowledgments

The authors are grateful to Y. Ihara, H. Ikeda, K. Ishida, M. Kato, Y. Kitaoka, Y. Kobayashi, C. Michioka, K. Miyake, Y. Ono, N. E. Phillips, H. Sakurai, M. Sato, M. Udagawa, Y. J. Uemura, K. Yamada, K. Yada, K. Yoshimura and G-q. Zheng for fruitful discussions. Numerical computation in this work was partly carried out at the Yukawa Institute Computer Facility. The present work has been partly supported by a Grant-In-Aid for Scientific Research from the Ministry of Education, Culture, Sport, Science and Technology of Japan.

1) F. Steglich, J. Aarts, C. D. Bredl, W. Lieke, D. Meschede, W. Franz, H. Schäfer, Phys. Rev. Lett. **43** (1979) 1892.
2) J. G. Bednorz and K. A. Müller, Z. Phys. B **64** (1986) 189.
3) For a review, K. Kanoda, Hyperfine Interactions **104** (1997) 235.

4) Y. Maeno, H. Hashimoto, K. Yoshida, S. NishiZaki, T. Fujita, J. G. Bednorz and F. Lichtenberg, Nature **372** (1994) 532.
5) K. Takada, H. Sakurai, E. Takayama-Muromachi, F. Izumi, R. A. Dilanian and T. Sasaki, Nature **422** (2003) 53.
6) M. Kato, C. Michioka, T. Waki, Y. Itoh, K. Yoshimura, K. Ishida, H. Sakurai, E. Takayama-Muromachi, K. Takada, T. Sasaki, cond-mat/0306036; C. Michioka, M. Kato, K. Yoshimura, K. Takada, H. Sakurai, E. Takayama-Muromachi and T. Sasaki, cond-mat/0403293.
7) Y. Kobayashi, M. Yokoi and M. Sato, J. Phys. Soc. Jpn. **72** (2003) 2161; 2453; J. Phys. Soc. Jpn. **74** (2005) 1800.
8) T. Fujimoto, G.-Q. Zheng, Y. Kitaoka, R. L. Meng, J. Cmaidalka and C. W. Chu, Phys. Rev. Lett. **92** (2004) 047004.
9) K. Ishida, Y. Ihara, Y. Maeno, C. Michioka, M. Kato, K. Yoshimura, K. Takada, T. Sasaki, H. Sakurai and E. Takayama-Muromachi, J. Phys. Soc. Jpn. **72** (2003) 3041; Y. Ihara, K. Ishida, C. Michioka, M. Kato, K. Yoshimura, K. Takada, T. Sasaki, H. Sakurai and E. Takayama-Muromachi, J. Phys. Soc. Jpn. **73** (2004) 2069.
10) W. Higemoto, K. Ohishi, A. Koda, S. R. Saha, R. Kadono, K. Ishida, K. Takada, K. Sakurai, E. Takayama-Muromachi and T. Sasaki, Phys. Rev. B **70** (2004) 134508.
11) Y. J. Uemura, P. L. Russo, A. T. Savici, C. R. Wiebe, G. J. MacDougall, G. M. Luke, M. Mochizuki, Y. Yanase, M. Ogata, M. L. Foo and R. J. Cava, cond-mat/0403031.
12) A. Kanigel, A. Keren, L. Patlagan, K. B. Chashka, P. King and A. Amato, Phys. Rev. Lett. **92** (2004) 257007.
13) H. D. Yang, J.-Y. Lin, C. P. Sun, Y. C. Kang, K. Takada, T. Sasaki, H. Sakurai and E. Takayama-Muromachi, Phys. Rev. B **71** (2005) 020504.
14) B. Lorenz, J. Cmaidalka, R. L. Meng and C. W. Chu, Physica C **402** (2004) 106.
15) N. Oeschler, R. A. Fisher, N. E. Phillips, J. E. Gordon, M. L. Foo and R. J. Cava, cond-mat/0409760.
16) M. Yokoi, H. Watanabe, Y. Mori, T. Moyoshi, Y. Kobayashi and M. Sato, J. Phys. Soc. Jpn. **73** (2004) 1297.
17) T. Sasaki, P. Badica, N. Yoneyama, K. Yamada, K. Togano and N. Kobayashi, J. Phys. Soc. Jpn. **73** (2004) 1131.
18) H. Sakurai, K. Takada, T. Sasaki and E. Takayama-Muromachi, cond-mat/0408426.
19) Y. Ihara, K. Ishida, C. Michioka, M. Kato, K. Yoshimura, K. Takada, T. Sasaki, H. Sakurai and E. Takayama-Muromachi, J. Phys. Soc. Jpn. **74** (2005) 867.
20) H. Sakurai, K. Takada, T. Sasaki and E. Takayama-Muromachi, preprint.
21) G. Baskaran, Phys. Rev. Lett. **91** (2003) 097003; D. Sa, M. Sardar and G. Baskaran, Phys. Rev. B **70** (2004) 104505.
22) B. Kumar and B. S. Shastry, Phys. Rev. B **68** (2003) 104508; Phys. Rev. B **69** (2004) 059901(E).
23) Q.-H. Wang, D.-H. Lee and P. A. Lee, Phys. Rev. B **69** (2003) 092504.
24) M. Ogata, J. Phys. Soc. Jpn. **72** (2003) 1839.
25) Y. Tanaka, Y. Yanase and M. Ogata, J. Phys. Soc. Jpn. **73** (2004) 319.
26) O. I. Motrunich and P. A. Lee, Phys. Rev. B **69** (2004) 214516; Phys. Rev. B **70** (2004) 024514.
27) G. Khaliullin, W. Koshibae and S. Maekawa, Phys. Rev. Lett. **93** (2004) 176401.
28) Y. Nisikawa, H. Ikeda and K. Yamada, J. Phys. Soc. Jpn. **73** (2004) 1127; H. Ikeda, Y. Nisikawa and K. Yamada, J. Phys. Soc. Jpn. **73** (2004) 17.
29) K. Yada and Y. Ono, unpublished.
30) K. Kuroki, Y. Tanaka and R. Arita, Phys. Rev. Lett. **93** (2004) 077001.
31) C. Honerkamp, Phys. Rev. B **68** (2003) 104510.
32) K. Kuroki, Y. Tanaka and R. Arita, Phys. Rev. B **71** (2005) 024506.
33) W. Koshibae and S. Maekawa, Phys. Rev. Lett. **91** (2003) 257003.
34) D. J. Singh, Phys. Rev. B **61** (2000) 13397; **68** (2003) 020503; M. D. Johannes and D. J. Singh, Phys. Rev. B **70** (2004) 014507.
35) J. Kuneš, K.-W. Lee and W. E. Pickett, cond-mat/0308388; K.-W. Lee, J. Kuneš and W. E. Pickett, Phys. Rev. B **70** (2004) 045104.
36) R. Arita, cond-mat/0502256.
37) M. Mochizuki, Y. Yanase and M. Ogata, Phys. Rev. Lett. **94** (2005) 147005.
38) Y. Yanase, M. Mochizuki and M. Ogata, J. Phys. Soc. Jpn. **74** (2005) 430.
39) A. T. Boothroyd, R. Coldea, D. A. Tennant, D. Prabhakaran and C. D. Frost, Phys. Rev. Lett. **92** (2004) 197201; L. M. Helme, A. T. Boothroyd, R. Coldea, D. Prabhakaran, D. A. Tennant, A. Hiess and J. Kulda, Phys. Rev. Lett. **94** (2005) 157206; S. P. Bayrakci, I. Mirebeau, P. Bourges, Y. Sidis, M. Enderle, J. Mesot, D. P. Chen, C. T. Lin and B. Keimer, Phys. Rev. Lett. **94** (2005) 157205.
40) T. Nomura and K. Yamada, J. Phys. Soc. Jpn. **69** (2000) 3678; J. Phys. Soc. Jpn. **71** (2002) 1993.
41) Y. Yanase, T. Jujo, T. Nomura, H. Ikeda, T. Hotta and K. Yamada, Phys. Rep. **387** (2004) 1.
42) D. F. Agterberg, T. M. Rice and M. Sigrist: Phys. Rev. Lett. **78** (1997) 3374.
43) A. J. Leggett: Rev. Mod. Phys. **47** (1975) 331.
44) M. Sigrist and K. Ueda, Rev. Mod. Phys. **63** (1991) 239.
45) H. Tou, K. Ishida and Y. Kitaoka, J. Phys. Soc. Jpn. **74** (2005) 1245.
46) P. W. Anderson, Phys. Rev. B **30** (1984) 4000.
47) K. Machida, T. Nishira, T. Ohmi, J. Phys. Soc. Jpn. **68** (1999) 3364 and references there in.
48) J. A. Sauls, Adv. Phys. **43** (1994) 153.
49) R. Joynt and L. Taillefer, Rev. Mod. Phys. **74** (2002) 235.
50) Y. Yanase and M. Ogata, J. Phys. Soc. Jpn. **72** (2003) 673.
51) K. K. Ng and M. Sigrist: Europhys. Lett. **49** (2000) 473.
52) C. Michioka and K. Yoshimura, private communication.
53) K. Takada, K. Fukuda, M. Osada, I. Nakai, F. Izumi, R. A. Dilanian, K. Kato, M. Takata, H. Sakurai, E. Takayama-Muromachi, T. Sasaki, J. Mater. Chem. **14** (2004) 1448.
54) M. Karppinen, I. Asako, T. Motohashi and H. Yamauchi, Chemistry of materials **16** (2004) 1693.
55) M. Mochizuki, Y. Yanase and M. Ogata, cond-mat/053233.
56) M. Z. Hasan, Y.-D. Chuang, A. Kuprin, Y. Kong, D. Qian, Y. W. Li, B. Mesler, Z. Hussain, A. V. Fedorov, R. Kimmerling, E. Rotenberg, K. Rossnagel, H. Koh, N. S. Rogado, M. L. Foo and R. J. Cava, Phys. Rev. Lett. **92** (2004) 246402.
57) H.-B. Yang, S.-C. Wang, A. K. P. Sekharan, H. Matsui, S. Souma, T. Sato, T. Takahashi, T. Takeuchi, J. C. Campuzano, R. Jin, B. C. Sales, D. Mandrus, Z. Wang and H. Ding, Phys. Rev. Lett. **92** (2004) 246403.
58) Y. Yanase, M. Mochizuki and M. Ogata, unpublished.
59) T. Nomura and K. Yamada, J. Phys. Soc. Jpn. **71** (2002) 404.
60) Y. Ihara and K. Ishida, K. Yoshimura, K. Takada, T. Sasaki, H. Sakurai and E. Takayama-Muromachi, cond-mat/0506751.
61) G.-Q. Zheng and Y. Kitaoka, private communication.
62) The role of a_{1g}-orbital can not be neglected when we consider the anisotropy of spin susceptibility precisely. We obtain $\chi_{ab}/\chi_c < 1$ in Fig. 8, however we find $\chi_{ab}/\chi_c > 1$ in the three-orbital model. M. Mochizuki, Y. Yanase and M. Ogata, unpublished.
63) H. Tou, Y. Kitaoka, K. Asayama, N. Kimura and Y. Onuki: Phys. Rev. Lett. **77** (1996) 1374; **80** (1998) 3129.
64) G. M. Luke, Y. Fudamoto, K. M. Kojima, M. I. Larkin, J. Merrin, B. Nachumi, Y. J. Uemura, Y. Maeno, Z. Q. Mao, Y. Mori, H. Nakamura and M. Sigrist: Nature **374** (1998) 558.
65) H. Murakawa, K. Ishida, K. Kitagawa, Z. Q. Mao, and Y. Maeno, Phys. Rev. Lett. **93** (2004) 167004.